

38. SIMULATION OF GEOLOGIC, HYDRODYNAMIC, AND THERMODYNAMIC DEVELOPMENT OF A SEDIMENT BASIN—A QUANTITATIVE APPROACH

M. Arif Yökler, C. Cornford, and D. Welte, Erdöl und Organische Geochemie, Kernforschungsanlage Jülich GmbH, Postfach 1913, 5170 Jülich, West Germany

ABSTRACT

This study determines the "quantitative" mass and energy transport in the sedimentary sequences of a basin. This is achieved by a one-dimensional deterministic model that accounts for the major mechanisms operating during sedimentation and compaction in the basin. Initial data consist of heat flux, initial physical and thermodynamic properties of sediments, paleobathymetric estimations, and sedimentation rate curve. The model then computes the two unknowns, hydraulic head (or pore pressure) and temperature, as a function of time and vertical distance. The physical and thermodynamic parameters are evaluated from the pressure and temperature calculations. These values are then put into the fluid and heat flow equations.

When applied to data from Holes 397 and 397A of DSDP Leg 47A, this model proves to be successful in simulating the geologic, hydrodynamic, and thermodynamic development of the sedimentary sequences. Effects of various parameters (e.g., geothermal gradient and slumping) are investigated using the model.

INTRODUCTION

A deterministic, dynamic model of fluid and heat flow in compacting sediments of a basin helps our understanding of the geologic, hydrodynamic, and thermodynamic development of a basin. A sedimentary basin is a complex system with mechanisms such as sedimentation, compaction, and subsidence operating within it. A "qualitative" understanding of these processes has been obtained through numerous temporal and spatial reconstructions of basin histories. Nevertheless, "quantitative" evaluation of the system and mechanisms operating therein are required to determine the validity of the theories, the hypothesis made, and the effectiveness of the various processes.

Knowledge of paleopressures and temperatures in a sedimentary basin are important for, and can place limits on, the solution of geologic, thermodynamic, mineralogic, geochemical, and hydrodynamic problems such as the following:

- a) Stratigraphic and sedimentologic development of a basin.
- b) Changes in the physical properties of fluids (density and viscosity) and sediments (compaction, permeability, porosity, etc.).
- c) Changes in thermal properties of fluids and sediments (heat capacity, thermal conductivity, etc.).
- d) Mineralogic changes effected by temperature and pressure.
- e) Generation, migration, and accumulation of hydrocarbons and other chemical constituents.

f) Fluid flow mechanisms, fluid flow directions and rates, and determination of abnormal fluid pressure zones.

Gibson (1958) studied the excess pressures assumed to be generated by a moving boundary condition, such as continuous sedimentation. Bredehoeft and Hanshaw (1968) examined pressure-producing mechanisms in a basin. They also used Gibson's equation to compute paleopressures. Sharp and Domenico (1976) studied energy transport in compacting sedimentary sequences.

This study is based on a one-dimensional fluid and heat flow model. Accumulation of sediments occurs upon an impermeable basement rock in a fluid environment and the thickness of sediments vary with time (Figure 1). In addition, the following assumptions are made:

- a) Darcy's law is valid.
- b) Fluid flow takes place vertically in thickening sedimentary sequences where both compaction and sedimentation occur.
- c) Geothermal heat flux is the only source of heat.
- d) Heat is distributed by conduction and forced convection (flow of water).

MATHEMATICAL FRAMEWORK

The differential equation for water flow in a compacting porous medium subject to continuous sedimentation is given by Gibson (1958). Gibson, however, derived this equation using the theory of one-dimensional compaction of a porous medium. The direct application to hydrodynamics should be made with great care. An-

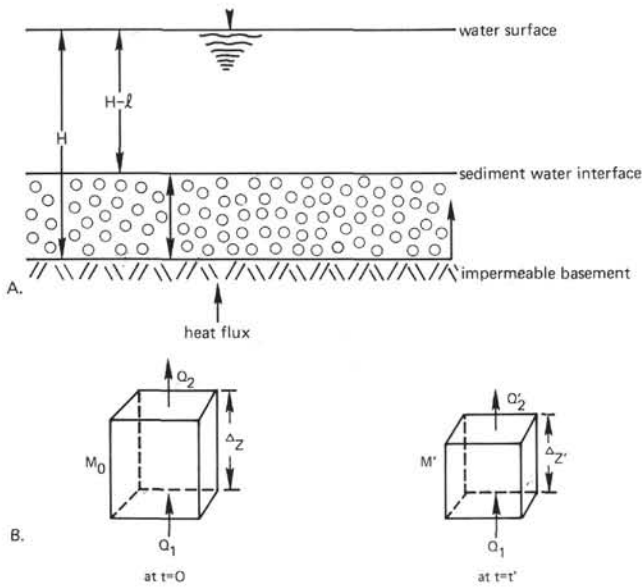


Figure 1. Schematic presentation of (A) the one-dimensional fluid and heat flow model, and (B) the volumetric approach for determining porosity (symbols are explained in text).

other equation is derived using conservation of mass, Darcy's law, and one-dimensional compaction under increasing overburden pressure. The continuity equation in non-steady state is

$$\left[\frac{\delta}{\delta z} \rho K \frac{\delta h}{\delta z} \right] \Delta z = \frac{\delta \Delta M}{\delta t} \quad (\text{Eq. 1})$$

where,

- h = hydraulic head, L
- k = hydraulic conductivity, L/T
- M = mass of fluid, M
- t = time, T
- z = vertical distance, L
- π = density of fluid, M/L³
- ΔM = $\pi \cdot \Theta \cdot \Delta z \cdot A$, A is base area (L²) and Θ is porosity.

Solid skeleton volume, ΔV_s , is considered incompressible,

$$d\Delta V_s = d[(1 - \theta) \Delta z, A] = 0$$

Taking partial derivative of ΔV_s with respect to time and arranging gives

$$\frac{\delta \theta}{\delta t} = \frac{(1 - \theta)}{\Delta z} \cdot \frac{\delta \Delta z}{\delta t}$$

but

$$\frac{1}{\Delta z} \cdot \frac{\delta \Delta z}{\delta t} = -\alpha \frac{\delta \sigma_z}{\delta t}$$

where

- α = compressibility of solid volume, LT²/M
- σ_z = effective stress, M/LT².

Therefore,

$$\frac{\delta \theta}{\delta t} = -\alpha(1 - \theta) \frac{\delta \sigma_z}{\delta t} \quad (\text{Eq. 2})$$

Taking partial derivative of ΔM with respect to time

$$\frac{\delta \Delta M}{\delta t} = \theta \Delta z \frac{\delta \rho}{\delta t} + \rho \Delta z \frac{\delta \theta}{\delta t} + \rho \theta \frac{\delta \Delta z}{\delta t} \quad (\text{Eq. 3})$$

and remembering that $\pi = \pi_0 e^{-\beta p}$, p is fluid pressure (M/LT²), B is compressibility of fluid (LT²/M), π_0 is initial density.

$$\frac{\delta \Delta M}{\delta t} = -\beta \rho_0 \theta \Delta z \frac{\delta p}{\delta t} - \rho \Delta z \alpha \frac{\delta \sigma_z}{\delta t} \quad (\text{Eq. 4})$$

From the definition of total stress, τ_z'

$$\sigma_z' = \sigma_z + p = \gamma_s(L - z) + \gamma_w(H - L)$$

where,

- H = water depth, L
- L = sediment thickness, L
- γ_s = specific weight of sediment, M/L²T²
- γ_w = specific weight of fluid, M/L²T².

Solving for τ_z' and putting in Equation 4

$$\frac{\delta \Delta M}{\delta t} = \left[\rho(\beta \theta + \alpha) \frac{\delta p}{\delta t} + \gamma_w \beta \alpha \rho (H - L) \frac{\delta p}{\delta t} - \rho \alpha (\gamma_s - \gamma_w) \frac{\delta L}{\delta t} - \gamma_w \alpha \frac{\delta H}{\delta t} \right] \Delta z \quad (\text{Eq. 5})$$

Hydraulic head is defined (Hubbert, 1940) as,

$$h = \int_{p_0}^p \frac{dp}{\gamma} + gz$$

Solving for p and replacing in Equations 4 and 1

$$\frac{\delta}{\delta z} K \frac{\delta h}{\delta z} = S_s \frac{\delta h}{\delta t} + \gamma_w^2 \beta \alpha (H - L) \frac{\delta h}{\delta t} - \alpha (\gamma_s - \gamma_w) \frac{\delta L}{\delta t} - \gamma_w \alpha \frac{\delta H}{\delta t} \quad (\text{Eq. 6})$$

where S_s is storativity,

$$S_s = \gamma \theta \beta \left(1 + \frac{\alpha}{\beta \theta} \right)$$

Making an analogy with unconfined flow systems (Hantush, 1964), Equation 6 is integrated along the vertical distance, z , from the base to the sediment-water interface.

The heat flow equation for the simultaneous transfer of heat both by conduction and forced convection (Stallman, 1963) is

$$\frac{\delta}{\delta z} K \frac{\delta T}{\delta z} - \rho_w C_{pw} \frac{\delta}{\delta z} (V_z T) + Q = C_{ws} \rho_{ws} \frac{\delta T}{\delta t} \quad (\text{Eq. 7})$$

where,

C_{pw}	=	specific heat of fluid, E/M°C
C_{ws}	=	specific heat of sediment, E/M°C
K	=	thermal conductivity, E/LT°C
Q	=	sink or source term, E/L ² T
T	=	temperature, °C
V_z	=	fluid flow in z direction, L/T
π_w	=	density of fluid, M/L ³
π_s	=	density of sediment, M/L ³

PARAMETERS OF THE MODEL

The parameters of this model can be considered in three groups.

Geologic Parameters

The definition of the geologic parameters requires a good knowledge of the sedimentology and geologic history of the basin. Lithology, sedimentation rate curve, and (if available) subsidence curve are needed to define the model. The stratigraphic column is treated as a continuum.

Hydrodynamic Parameters

The hydrodynamic parameters of the model are K , hydraulic conductivity, and S_s , specific storage, defined as

$$K = \frac{k \rho_w g}{w}$$

$$S_s = \rho_w g (\alpha + \theta \beta)$$

where,

g	=	gravity, L/T ²
k	=	permeability, L ²
w	=	dynamic viscosity, M/LT.

All these variables change with space and time as a function of pressure and temperature. The variables are handled "semi-explicitly" in the model using the following relationships.

Porosity is determined in two different ways:

1) Change in porosity with respect to compressibility of the solid skeleton and rate of change in effective stress,

$$\frac{\delta \theta}{\delta t} = -\alpha (1 - \theta) \frac{\delta \sigma_z}{\delta t}$$

2) Change in porosity with respect to variations of water volume at every time step is considered. This is called the "volumetric approach," as shown in Figure 1B, where

M_0, M'	=	Mass of water at times zero and t'
Q_1, Q_2	=	Rate of water flow in and out of the unit volume at time zero
Q_1', Q_2'	=	Rate of water flow in and out of the unit volume at time t'
$\Delta z, \Delta z'$	=	Height of the unit volume at times zero and t' .

Ratio of M_0 to M' is

$$R_m = \frac{M_0}{M'} = \frac{\rho \theta \Delta z \cdot A}{\rho' \theta' \Delta z' \cdot A} = \frac{\rho \theta \Delta z}{\rho' \theta' \Delta z'} \quad (\text{Eq. 8})$$

π , θ , and Δz are values at time zero and π' , θ' and $\Delta z'$ are at time t' . A is the base area. Ratio of initial solid volume to volume at t' is

$$R_s = \frac{\Delta V_s}{\Delta V_s'} = \frac{(1 - \theta) \Delta z \cdot A}{(1 - \theta') \Delta z' \cdot A} = \frac{(1 - \theta) \Delta z}{(1 - \theta') \Delta z'} = 1$$

Therefore,

$$\Delta z' = \frac{(1 - \theta)}{(1 - \theta')} \Delta z \quad (\text{Eq. 9})$$

Replacing $\Delta z'$ in Equation 8 and solving for θ'

$$\theta' = \frac{\theta \rho M}{\rho' M_0 - \rho' \theta M_0 + \theta \rho M'} \quad (\text{Eq. 10})$$

Since the right side of Equation 10 is easily computed, θ' values are determined from this equation. Then, θ'

is replaced in Equation 9 and $\Delta z'$ values are calculated. The difference

$$C = \Delta z - \Delta z' \quad (\text{Eq. 11})$$

gives the amount of compaction of a unit of sediment for each time step.

Permeability is determined from the computed porosity values and permeability versus porosity curves (Pirson, 1963; Magara, 1974; Chilingarian et al., 1976).

Fluid density is computed by

$$\rho_w = \rho_{wo} [1 + \beta_p(p - p_o) + \beta_T(T - T_o)]$$

where,

B_p = coefficient of pressure fluid volume expansion

B_T = coefficient of thermal fluid volume expansion.

Sediment density is calculated from

$$\rho_s = \theta \rho_w + (1 - \theta) \rho_r$$

where,

ρ_r = density of rock.

Fluid viscosity is assumed to vary as (corrected from Sharp and Domenico, 1976)

$$\mu = (5.3 + 3.8A - 0.26A^3)^{-1}$$

where

$$A = (T - 150^\circ\text{C}) / 100^\circ\text{C}$$

Thermodynamic Parameters

The thermodynamic parameters of the model are K , thermal conductivity, and C , heat capacity.

Thermal conductivity of sediment is approximated by (Lewis and Rose, 1970)

$$K_s = K_r (K_w / K_r)^\theta$$

where,

K_r, K_s, K_w = thermal conductivities of rock, sediment, and fluid (respectively).

Heat capacity of sediment is determined by

$$C_s = (1 - \theta) C_r [1 + \lambda_r(T - T_o)] + \theta C_w [1 + \lambda_w(T - T_o)]$$

where,

C_r, C_s, C_w = heat capacities of rock, sediment, and fluid (respectively)

λ_r, λ_w = constants describing temperature variation of heat capacities of rocks and fluids found from thermo-physical tables.

APPLICATION OF THE MODEL TO DSDP SITE 397

Sedimentation at Deep Sea Drilling Project Site 397 is modeled and the resulting trends are compared with the shipboard data.

General Geology

Site 397 was drilled into continental rise sediments off the west coast of North Africa about 110 km south of the Canary Islands (Figure 2). The hole, continuously cored to 1453 meters penetrated a thick Pleistocene to Miocene section overlying Lower Cretaceous mudstones (Figure 3). Only the Tertiary section to 1300 meters modeled in this study.

The Tertiary section is composed of two major sediment intervals. From the ocean floor to 752 meters, (Recent to middle Miocene) the sediments are dominated by hemipelagic nannofossil oozes and chalks which are subdivided into three lithologic units. These skeletal products of high bioproductivity represent autochthonous sedimentation in this rise setting (Figure 4). From 752 to 1300 meters, an allochthonous (early Miocene), fourth lithologic unit of slumps and turbidites was found (Figure 4). Sediments in this interval are characterized by erratically interbedded clays, silts, sands, and pebbly mudstones. They are thought to be derived from the continental shelf edge via mass transport in canyons that dissect the slope in this region. Several minor unconformities were identified in this section. One, of 2.0 m.y. duration, occurs at 674 meters. A shorter one, at 250 meters, exhibit changes in physical properties, between sediments above and below the disconformity plane.

Computer Modeling Of Site 397 Data Compilation

The geothermal gradients, lithologic descriptions, paleobathymetric estimation, and sedimentation rate curve were obtained from the post-cruise reports. The data are given in Table 1. Uncorrected sedimentation rate curve is given in Figure 5. An initial correction is made to the sedimentation rates to account for compaction. After correction, the Pliocene/Quaternary sedimentation is approximately 96 m/m.y., the upper Miocene is 62 m/m.y., and the unconformity below the middle Miocene is 64 m/m.y. The early Miocene sedimentation rate is estimated to be 182 m/m.y. These values, however, are initial corrections; further correction is discussed later.

MODEL FORMULATION

Equations 5 and 6 are solved to compute water and heat flow in the system. The equations are solved by finite-difference techniques (Yükler, 1976). A grid spacing of 3 meters and a time interval of 100,000 years are used. When the hydraulic head (or pore pressure) and temperature values are calculated, the parameters are adjusted and replaced in Equations 5 and 6. Thus, the parameters of the equations are handled semi-explicitly. Compaction values are also computed

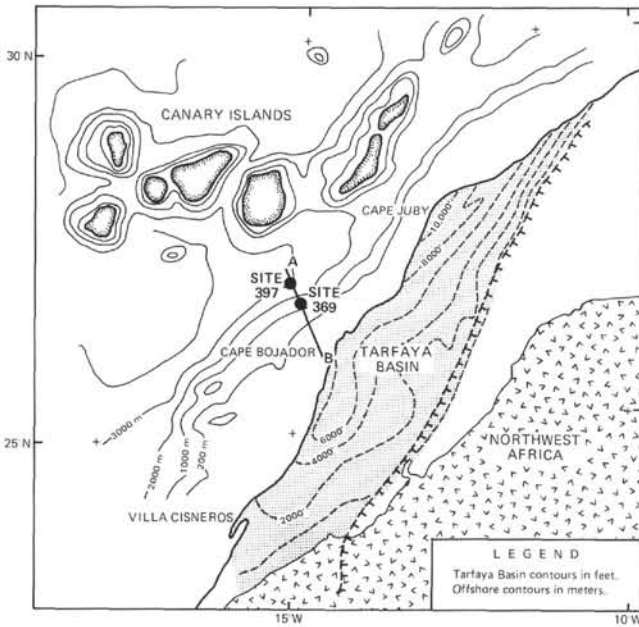


Figure 2. Topography near Site 397 with sediment isopachs for onshore portion of Tarfaya Basin.

at this level and an adjustment to the depth of accumulated sediment is made. Then the equations are solved for a better determination of hydraulic head and temperature. The model prints the results after every million years. The computations halt after 21 million years, i.e., at the present.

ANALYSIS OF RESULTS

The hydraulic head, pore pressure, temperature, and physical and thermodynamic parameters of the system are calculated as a function of space (depth) and time. The results are compared with the experimentally determined values of porosity, density, and downhole temperature. Several computer runs were made until the difference between computed and experimental values fell within acceptable limits.

From the large number of optimization runs, the effects of three variables were tested. The results are discussed as the following cases. In Case 1, the sedimentation rate curve is corrected in accordance with the core descriptions; initial porosity and density, and geothermal gradient are as in Table 1. Case 2 is similar to Case 1, but uniform initial porosity (that of Unit 1) is assumed throughout; the sedimentation rate curve is corrected mainly by adding additional slumps. Case 3 is similar to Case 2, but varying the geothermal gradient.

Case 1: Figure 6 gives the computed and observed porosity curves as a function of depth. For clarity, computed points are shown only every 30 meters, although the trend follows the values calculated every 3 meters. The "observed" curve is the weighted mean of the experimental points which are plotted as open circles in Figure 6. Considerable scatter, shown in the measured points, reflects the heterogeneous nature of the sediments at this site and, in some cases, drilling disturbance. The relative accuracy of the physical property

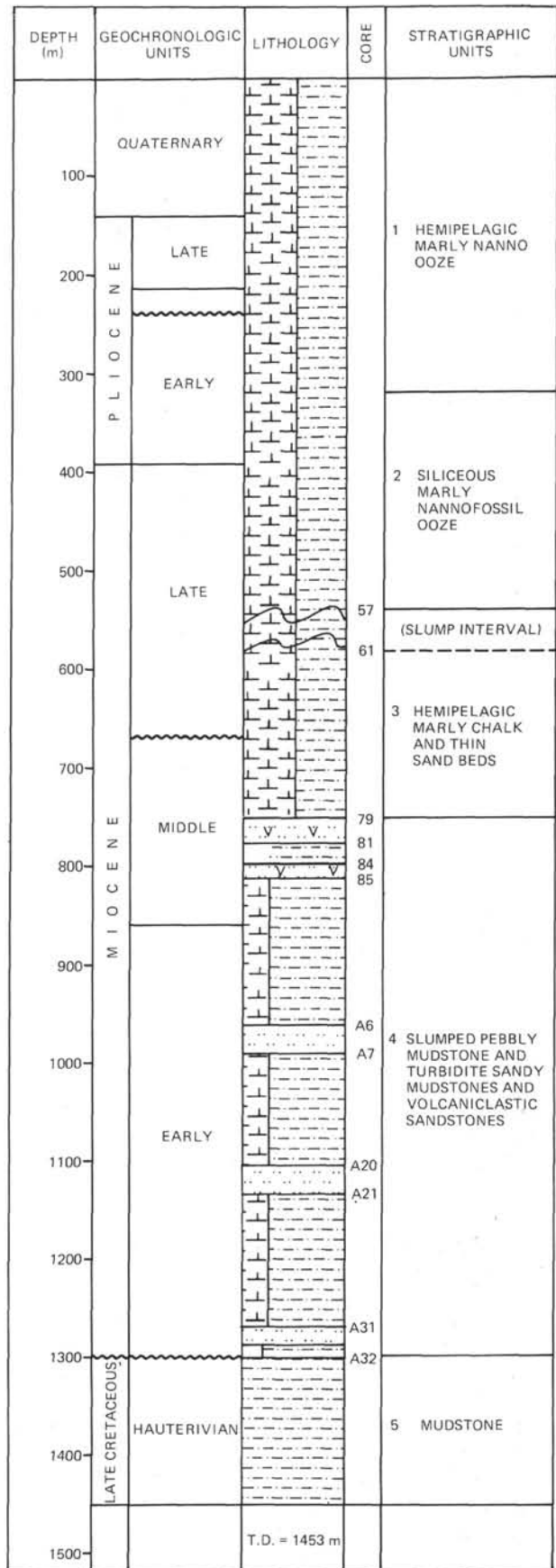


Figure 3. Lithography and biostratigraphy at Site 397.

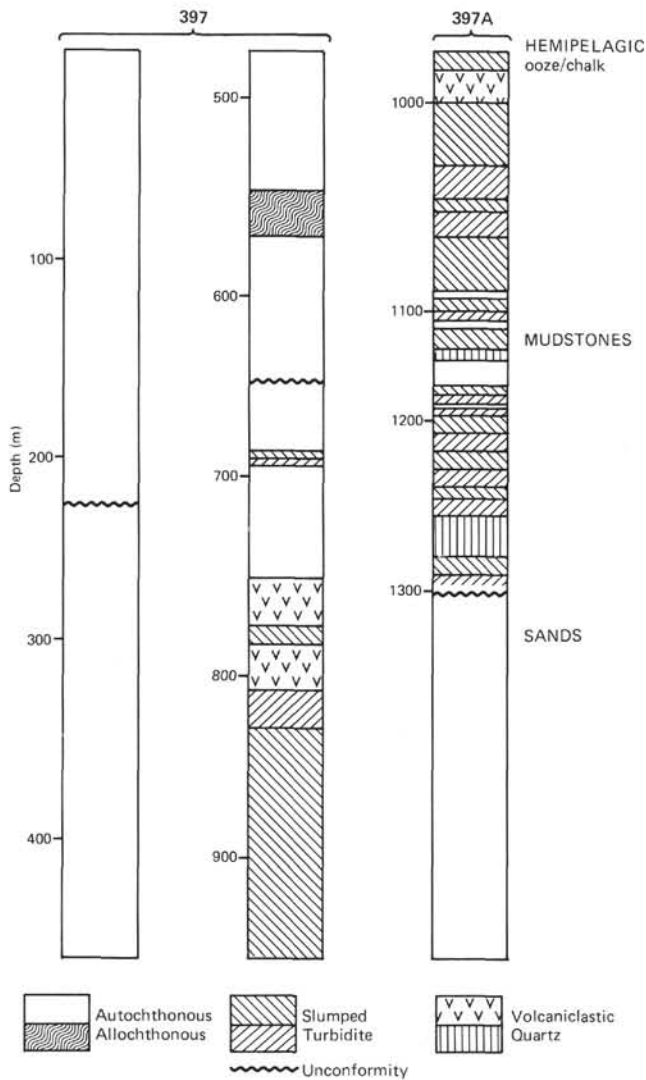


Figure 4. Symbolic representation of dominant lithology with 3-meter intervals at DSDP Site 397.

values was compared with gamma ray attenuation measurements in the shipboard report; the agreement of the finding was good. The computed and observed porosity trends of Figure 6 show close correlation both in slope and in detailed points of inflection. The trends deviate by an average percentage error of less than ± 2 per cent porosity. A similar general and detailed fit was obtained for the density values.

Two interesting features are shown in Figure 6, superimposed on the normal reduction in porosity with depth. Firstly the disconformities modeled at 235 meters and 650 meters show reduced porosities in the sediments deposited on the plane of the disconformity. A similar feature is observed at the base of the section (1300 m) where underlying sediments were modeled as an impermeable basement. Secondly, a reduction in porosity is also seen at and below the slump horizons, e.g., between 420 and 480 meters. Slumping appears to squeeze the underlying sediments.

Figure 7 illustrates the computed temperature profile. This matches well with the observed values: at 360 meters depth, $T_{obs} = 19.5 \pm 0.50^\circ\text{C}$ and $T_{comp} = 19.70^\circ\text{C}$; at 447 meters, $T_{obs} = 22.50 \pm 0.25^\circ\text{C}$ and $T_{comp} = 23.01^\circ\text{C}$. The computed geothermal gradient is $43.78^\circ\text{C}/\text{km}$ from 0 to 410 meters $35.56^\circ\text{C}/\text{km}$ from 410 to 1300 meters (Figure 7).

To obtain this fit of porosity, density, and temperature data, the sedimentation rate curve was revised within reasonable limits. The revised curve is shown in Figure 8.

Case 2: Slumps were encountered in the two major Neogene stratigraphic intervals at Site 397 (Figures 3 and 4). The effect of reducing the "background" sedimentation rate and compensating in thickness by introducing instantaneous slumps was therefore modeled, and the results are shown in Figures 9 and 10. The corrected sedimentation rate is given in Figure 11. Since the thickness of individual slumps could not be estimated from DSDP core descriptions, the horizons and depth used were chosen to give the best fit to the experimental trends.

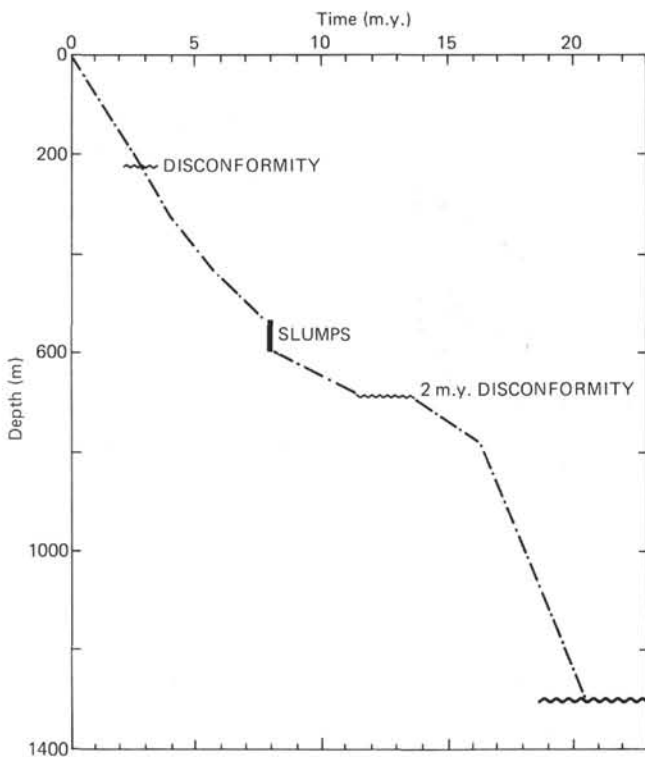
Case 2 is different from Case 1 in that, by comparison with the experimental curves, higher porosities and lower densities are found, particularly in the lower part of the section (Figures 9 and 10). Higher porosities and lower densities can be due to either over-estimation of the initial porosities or due to lateral water movement, a limitation of the one-dimensional model. In both cases, reduced compaction in the simulated sequences accounts for over-estimation of porosity and under-estimation of density. The model is one dimensional (only considers changes along the vertical axis), thus neglecting lateral water and heat flow.

The inclination of the seismic horizons (Figure 12) suggests that water and heat flow can be lateral as well as vertical, especially below seismic horizon number 4. However, the dips of the seismic horizons are exaggerated in Figure 12 and are probably not greater than 3 per cent. The results of lateral water flow may be indicated on the porosity plot (Figure 9) by a divergence of the experimental and calculated trends below 390 meters. Water is not permitted to escape laterally from the sedimentary sequences by the model, which results in higher porosities. The same argument can account for the divergent trends for densities (Figure 10). Nevertheless, the one-dimensional approach appears applicable in this case since the errors between computed and observed values are small.

Case 3: The effect of the temperature on the physical and thermodynamic properties of sediments has also been modeled. The heat flux was varied such that a change of $\pm 5^\circ\text{C}/\text{km}$ was observed in the geothermal gradients. The model run with the lower heat flux results in 1400 meters of sediments, 100 meters of sediment more than actually encountered; the run with the higher heat flux resulted in 1236 meters of sediments, 64 meters sediments less. These results indicate that a higher rate of compaction occurs for higher heat flux. The porosity values and the temperature profiles for

TABLE 1
Initial Data Used to Model DSDP Site 397

Property	Value	Remarks
Pressure coefficient of expansion of fluid phase	$B_p = 0.0$	Pressure effect is assumed negligible
Temperature coefficient of expansion of fluid phase	$B_T = -5 \times 10^{-4}/^\circ\text{C}$	From Harlow and Pracht, 1972
Compressibility of solid volume	$\alpha = 7.14 \times 10^{-5} - 7.14 \times 10^{-7} \text{ (kg/cm}^2\text{)}$	As an initial guess α is varied two order of magnitudes from $\theta_0 = 0.68$ to $\theta = 0.25$
Density of fluid	$\xi_w = 1.004 \text{ g/cm}^3$	Initial value
Density of solids of Unit I	$\xi'_r = 2.550 \text{ g/cm}^3$	Initial value modified from measurements
Density of solids of Unit II	$\xi''_r = 2.610 \text{ g/cm}^3$	Initial value modified from measurements
Density of sediment	$\xi_s = \Theta \xi_w + (1 - \Theta) \xi'_r$	Computed from θ , ξ_w , ξ'_r and ξ''_r
Fluid dynamic viscosity	$\omega = 1.06 \text{ certipoise}$	Initial value, but later computed from viscosity equation
Geothermal gradient	$G = 42^\circ\text{C/km}$	Initial value, later adjusted
Gravity	$g = 9.8 \text{ m/sec}^2$	
Heat capacity of fluid phase	$C_w = 1.008 \text{ cal/g } ^\circ\text{C}$	Estimated from Kappelmeyer and Haenel, 1974
Heat capacity of Unit I	$C'_r = 0.214 \text{ cal/g } ^\circ\text{C}$	Estimated from Kappelmeyer and Haenel, 1974
Heat capacity of Unit II	$C''_r = 0.209 \text{ cal/g } ^\circ\text{C}$	Estimated from Kappelmeyer and Haenel, 1974
Initial porosity of Unit I	$\theta'_0 = 0.68$	From measurements
Initial porosity of Unit II	$\theta''_0 = 0.57$	From measurements
Initial water depth	$H = 4000 \text{ m}$	Estimate from available data
Temperature (initial sediment-water interface)	$T_0 = 4^\circ\text{C}$	
Thermal conductivity of fluid	$K_w = 1.348 \times 10^{-3} \text{ (cal/cm. sec } ^\circ\text{C)}$	Estimated from Kappelmeyer and Haenel, 1974
Thermal conductivity of Unit I	$K'_r = 5.100 \times 10^{-3} \text{ (cal/cm. sec } ^\circ\text{C)}$	Estimated from Kappelmeyer and Haenel, 1974
Thermal conductivity of Unit II	$K''_r = 6.300 \times 10^{-3} \text{ (cal/cm. sec } ^\circ\text{C)}$	Estimated from Kappelmeyer and Haenel, 1974


Figure 5. Uncorrected sedimentation rate curve, DSDP Site 397.

the three gradients are given in Figures 13 and 14, respectively. These curves clearly indicate that the geothermal gradient affects the compaction (hence, the apparent sedimentation rate), thereby influencing the subsidence history.

CONCLUSIONS

A new differential equation is derived for water flow in a compacting porous medium with a moving boundary condition. This equation is solved simultaneously with the well-known heat flow equation (conduction and convection). The necessary adjustments are made to the parameters of the system with changes in pressure and temperature.

The one-dimensional, deterministic, dynamic model is applied successfully to DSDP Site 397. The model results match the observed physical properties and temperature. Discrepancies between the computed and experimental curves for density and porosity could be explained if lateral water movement was postulated, suggesting the use of a three-dimensional approach. In the absence of lateral flow, the match is obtained by varying initial porosities (within reliable limits), putting in slumps (to compact the system more), and changing heat flux and sedimentation rates. The optimum combination of the above changes gave the best fit for depth, physical and thermodynamic properties, and temperature measurement. No unique solution is

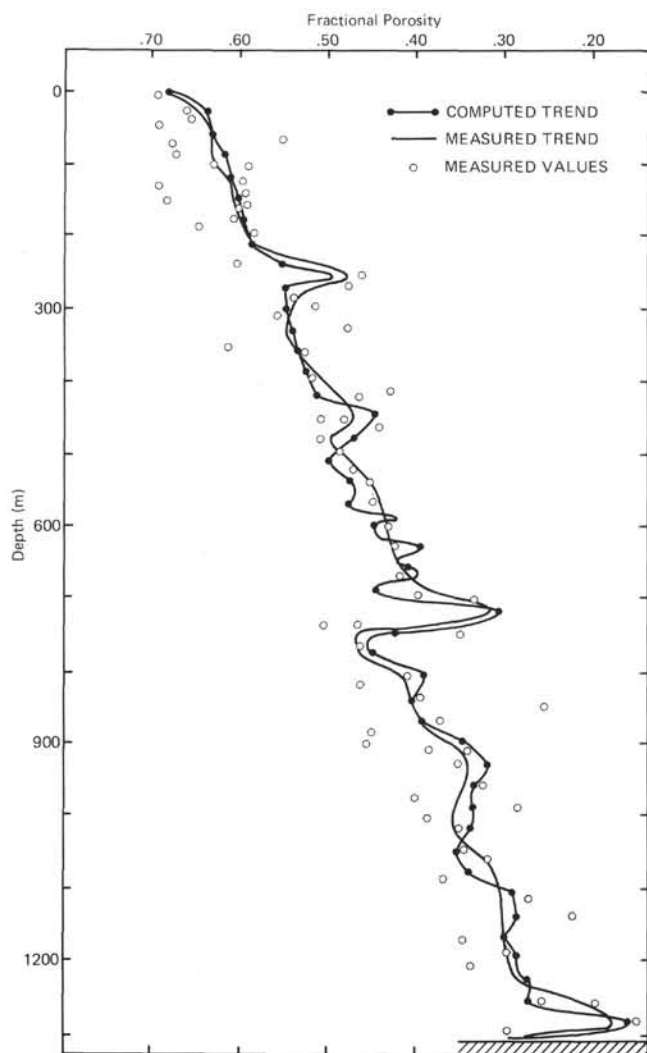


Figure 6. Depth trends for computed and observed porosity for Case 1.

claimed. The results place limits on the paleopressures and paleotemperatures at this site.

Temperature was found to have a great effect on the physical properties, especially porosity and density. Higher temperatures increase water flow, which in turn increases compaction, decreases porosity, and increases density. The effect of temperature on the porosity versus depth relationship will be discussed in detail in another paper.

ACKNOWLEDGMENTS

We acknowledge the use of the privileged information produced by the shipboard party of DSDP Leg 47, in particular the physical property measurements made by Greg Mountain.

REFERENCES

Bredehoeft, J. D. and Hanshaw, B. B., 1968. On the maintenance of anomalous fluid pressure: I. Thick sedimentary sequences, *Geol. Soc. Am. Bull.*, v. 79, p. 1097-1106.
 Chilingarian, G. V., Wolf, K. H., and Allen, D. R., 1976. Introduction. In Chilingarian, G. V. and Wolf, K. H. (Eds.), *Compaction of coarse-grained sediments*: New York (Elsevier Scientific Publ. Comp.), p. 1-42.

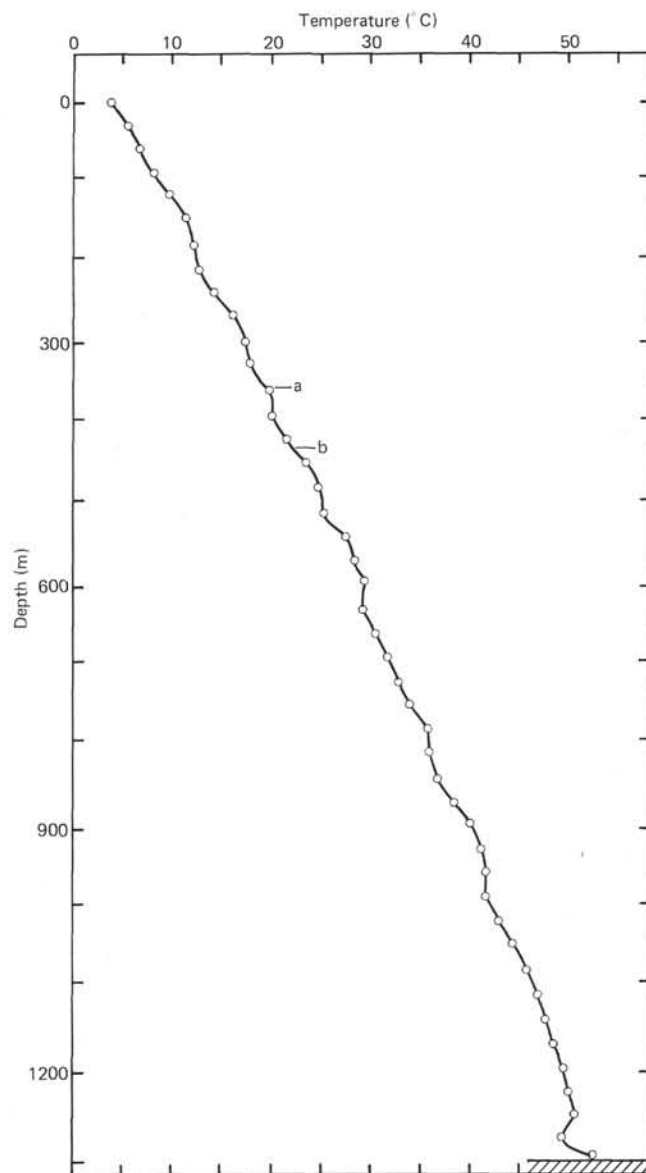


Figure 7. Computed temperature profile for Case 1; (A) (at 360 m depth) indicates $T_{obs} = 19.5 \pm 0.50^\circ\text{C}$ and $T_{comp} = 19.70^\circ\text{C}$ and (B) (at 447 m) indicates $T_{obs} = 22.5 \pm 0.25^\circ\text{C}$ and $T_{comp} = 23.01^\circ\text{C}$.

Gibson, R. E., 1958. The progress of consolidation in a clay layer increasing in thickness with time, *Geotechnique*, v. 8, p. 172-182.
 Hantush, M. S., 1964. Hydraulics of wells. In Chow, V.T. (Ed.), *Advances in hydroscience*: New York (Academic Press), p. 281-432.
 Harlow, F. H. and Pracht, W. E., 1972. A theoretical study of geothermal energy extraction, *J. Geophys. Res.*, v. 77, p. 7038-7048.
 Hubbert, M. K., 1940. The theory of groundwater motion, *J. Geol.*, v. 48, p. 785-944.
 Kappelmeyer, O. and Haenel, R., 1974. Geothermics with special references to application. In Rosenbach, O., and Morelli, C. (Eds.), *Geoexploration Monographs*, Series 1, No. 4, Gebrüder Borntraeger, Paul Christian KG.
 Lewis, C. R. and Rose, S. C., 1970. A theory relating high temperatures and overpressures, *J. Petrol. Tech.*, v. 22, p. 11-16.

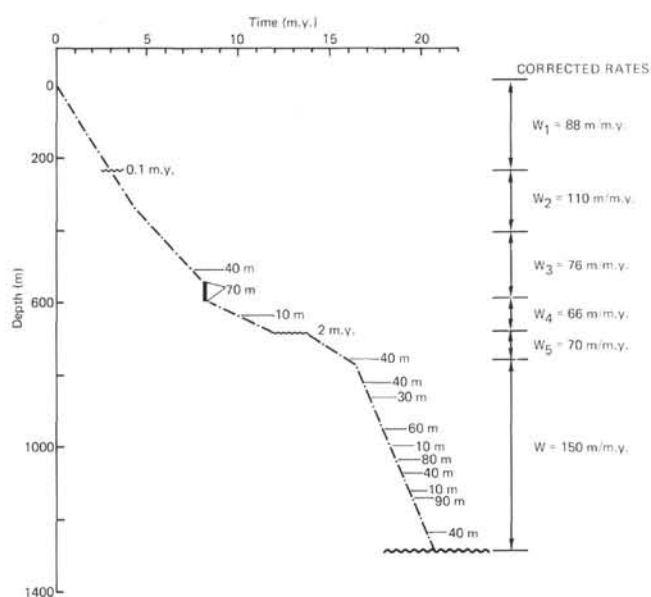


Figure 8. Corrected sedimentation rate curve from Case 1. (Meters indicated on the curve represent the thickness and position of slumped horizons used in Case 1.)

Magara, k., 1974. Compaction and fluid migration in cretaceous of Western Canada, Geol. Survey of Canada Publ.

Pirson, J.S., 1963. *Handbook of well log analysis for oil and gas formation evaluation*: Englewood-Cliffs, N. J. (Prentice-Hall, Inc.).

Sharp J. M. Jr. and Domenico, P. A., 1976. Energy transport in thick sequences of compacting sediment., *Geol. Soc. Am. Bull.*, v. 87, p. 390-400.

Stallman, R. W., 1963. Computation of ground-water velocity from temperature data. In Bentall, R. (Ed.), *Methods of collecting and interpreting ground-water data*: U. S. Geol. Survey Water Supply Paper 1544-H, p. 36-46.

Yüklér, M. A., 1976. Analysis of error in groundwater modeling, Ph.D. Thesis, University of Kansas.

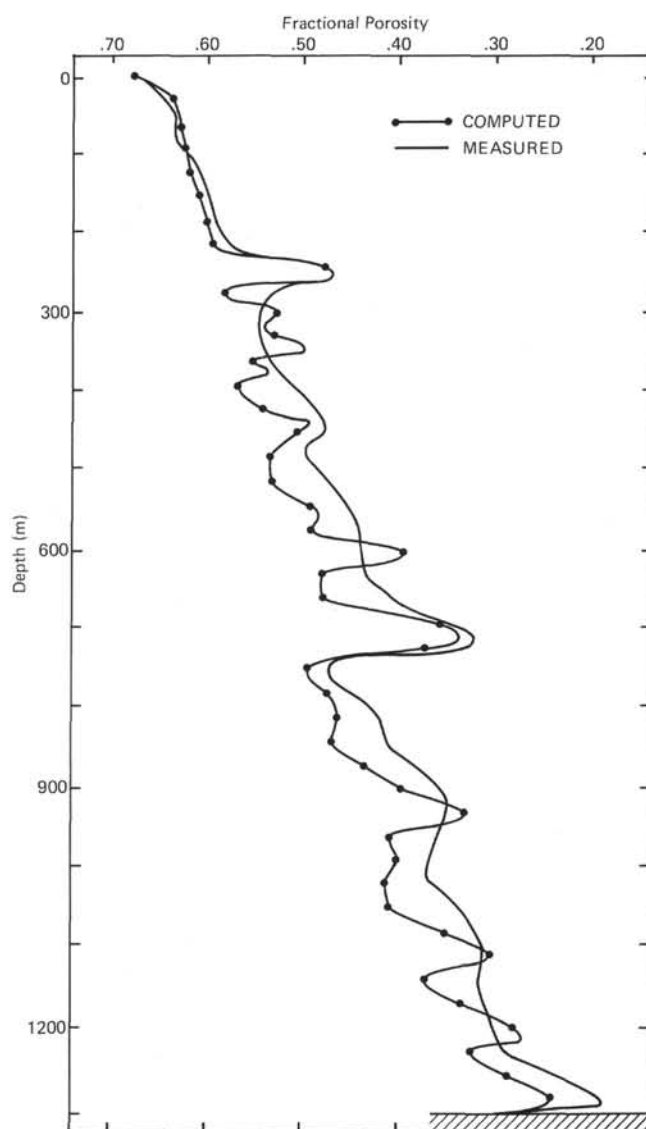


Figure 9. Depth trends for computed and observed porosity values in Case 2.

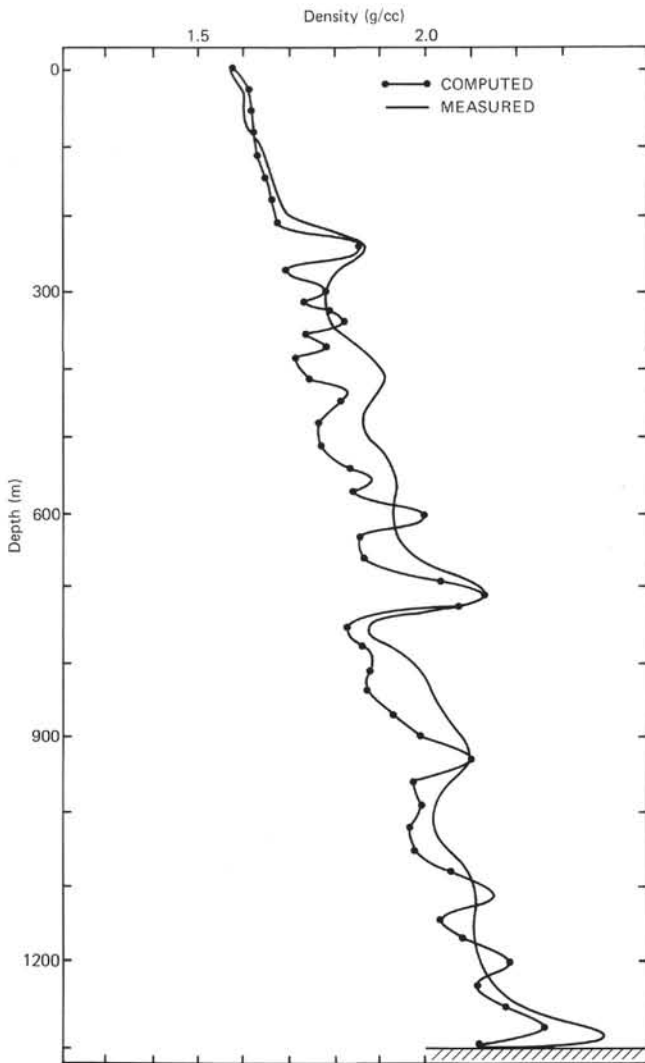


Figure 10. Depth trends for computed and observed density values in Case 2.

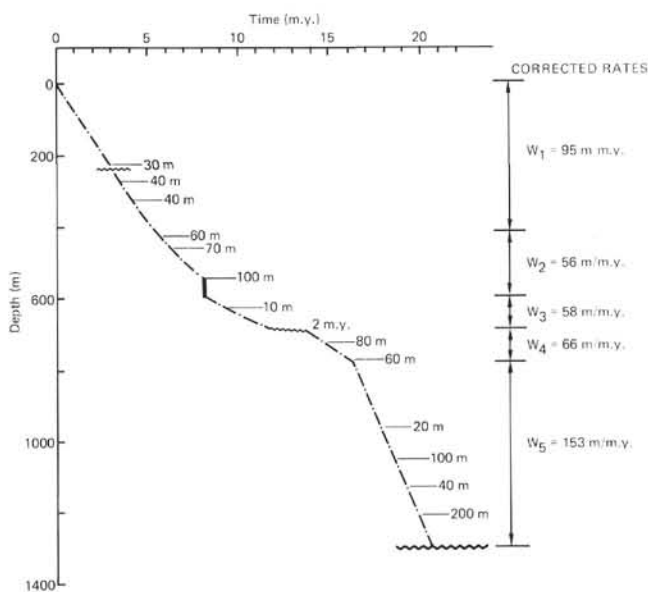


Figure 11. Corrected sedimentation rate curve in Case 2. Instantaneous slumps are introduced to match the physical and thermal properties.

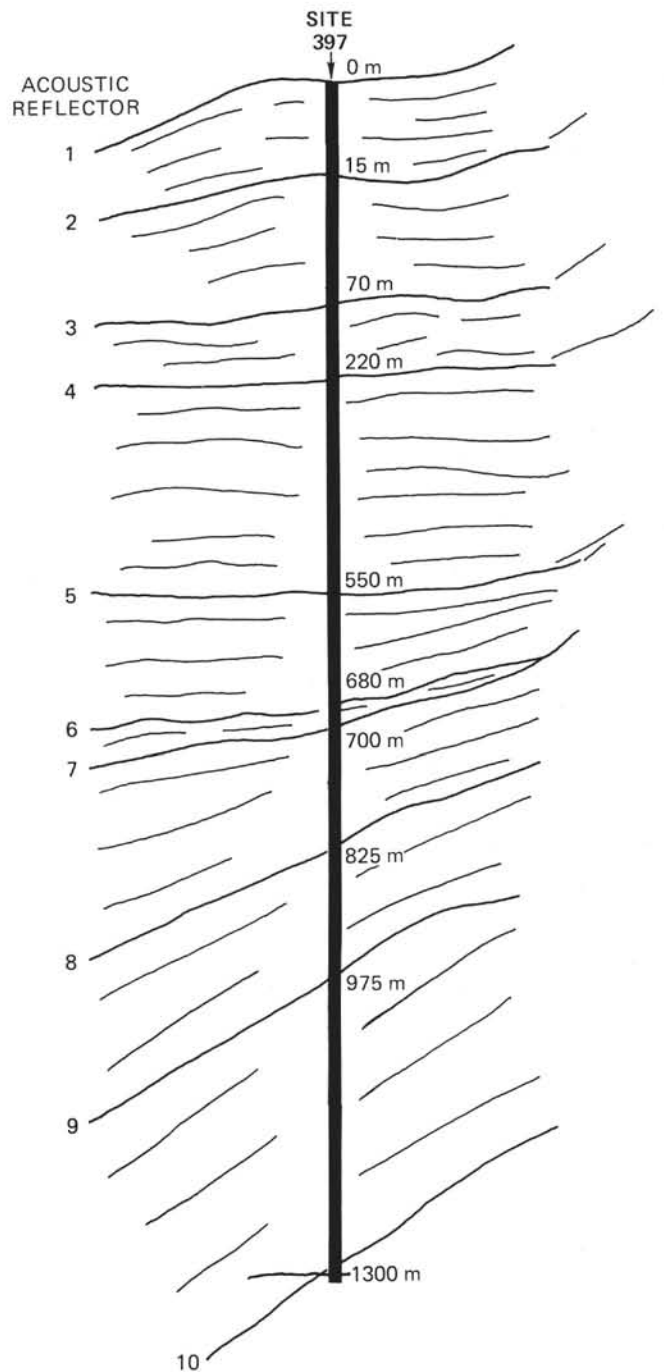


Figure 12. Seismic horizons recorded at Site 397.

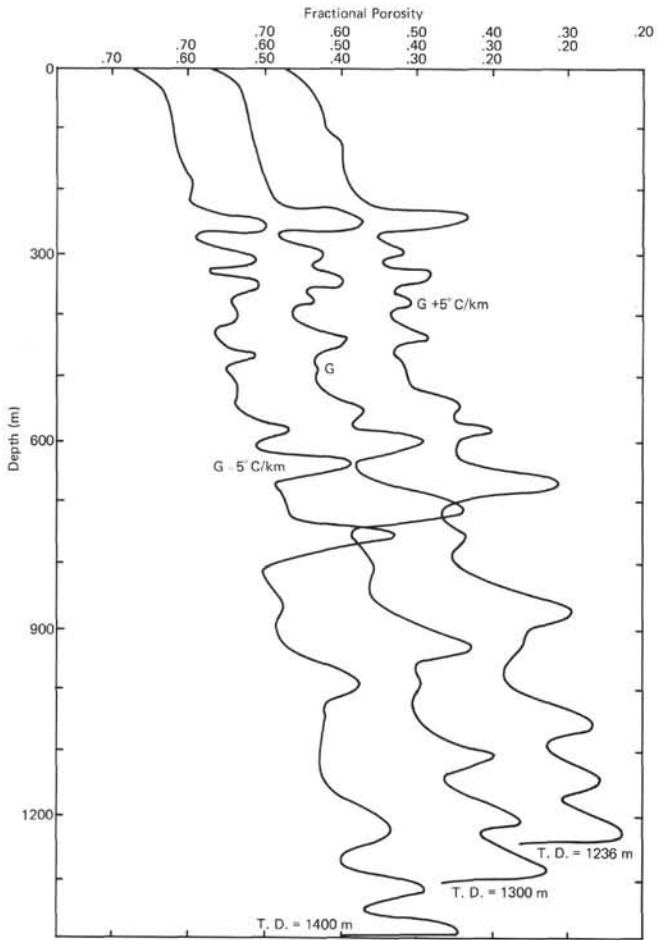


Figure 13. Effect of geothermal gradient (G) on porosity versus depth relationships.

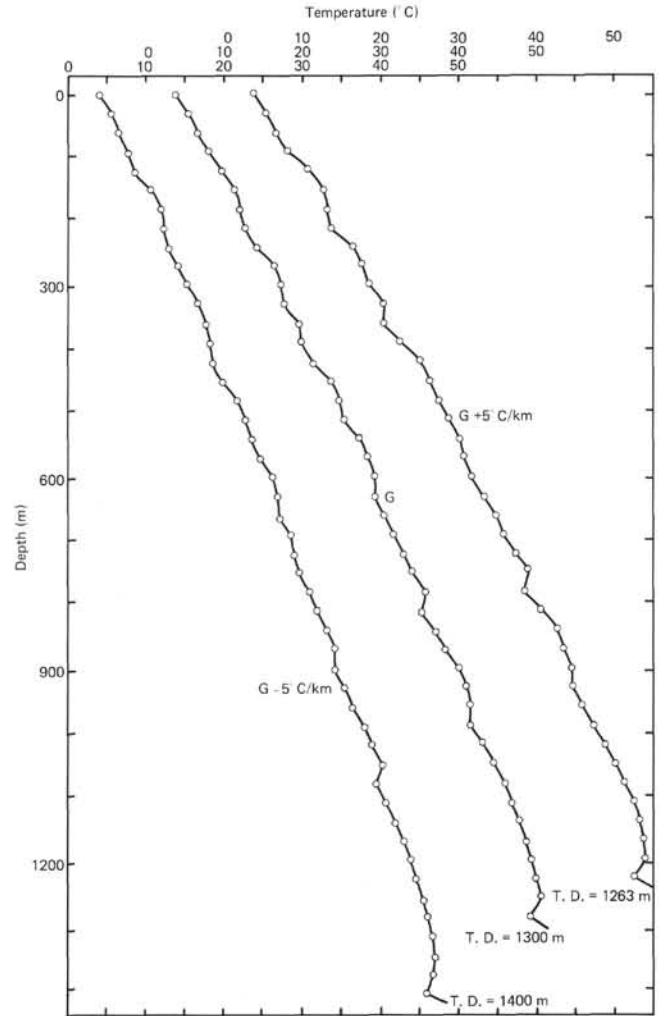


Figure 14. Effect of variable heat flux on the temperature profiles.